RSC Advances

PAPER

View Article Online
View Journal | View Issue

Cite this: *RSC Adv.*, 2018, **8**, 28978

High electrochemical performance of nanocrystallized carbon-coated $LiFePO_4$ modified by tris(pentafluorophenyl) borane as a cathode material for lithium-ion batteries

Yifang Wu, *[a] Shaokun Chong,[b] Yongning Liu,[b] ShengWu Guo,[b] Pengwei Wang,[a] Lifeng Bai[a] and Chengshan Li[a]

Received 15th May 2018
Accepted 18th July 2018

DOI: 10.1039/c8ra04119a

rsc.li/rsc-advances

Tris(pentafluorophenyl) borane ($C_{18}BF_{15}$) was first adopted as a boron source, which clearly demonstrated its modification effects. XPS and EDX mapping proved that boron can be successfully doped into a carbon layer. The high number of defects in the carbon induced by boron was demonstrated *via* Raman spectroscopy and thus, the electric conductivity of $LiFePO_4$ was greatly enhanced. The boron-doped composite possessed a higher specific discharge capacity and rate capability than the undoped sample. For instance, the reversible specific capacity for the boron-doped cathode reached 165.8 mA h g^{-1} at 0.5C, which was almost close to its theoretical capacity (166 mA h g^{-1}). Even at a high rate of 5C, it still possessed a high specific capacity of 124.8 mA h g^{-1}. This provides for the possibility that boron-doped carbon-coated $LiFePO_4$ cathodes may deliver high energy and power density for rechargeable lithium-ion batteries.

1. Introduction

Lithium-ion batteries (LIBs) play a significant role in a variety of portable electronic devices including electrical grids and electric and hybrid vehicles. Since the cathode material constitutes 30–40% of the manufacturing costs of a Li-ion battery, it is a key material to determine the safety, performance, cost and cycle life of LIB. Lithium iron phosphate ($LiFePO_4$) has attracted the most interest because of its environmental friendliness, low material cost, high safety, long cycle life, acceptable operating voltage (3.4 V *vs.* Li^+/Li), and reasonable theoretical capacity of 170 mA h g^{-1}. The major challenge for $LiFePO_4$ is its sluggish rate performance due to its intrinsically low electrical conductivity and lithium-ion diffusion coefficient. Therefore, obtaining further improvements for achieving high rate performance is still a challenge that must be solved for $LiFePO_4$ before it can be used to satisfy the demands of power devices.

To improve the rate capability of $LiFePO_4$, numerous efforts have been made including conductive coatings,[1–5] elemental doping[6–8] and nanoscale optimization.[9,10] Of all these strategies, reducing $LiFePO_4$ grains to the nanoscale has been demonstrated to be highly effective because it shortens the migration distance of lithium ions. Moreover, elemental doping has significant effect on the electronic conductivity of the carbon layers in LIBs. So far, doping with nitrogen,[11–13] sulfur,[14–16] phosphorus[17] and boron[18–20] has been studied, and it has demonstrated improved electrochemical properties for the cathode materials. Boron atoms have a unique characteristic: they can substitute carbon atoms[21] in the crystal lattice and serve as acceptor sites for electrons *via* their particular electronic structures.[22] In comparison to pristine materials, boron-doped carbon coatings possess enhanced electric conductivity as dopants can provide more electron carriers in the conduction band.

In this study, a boron-doped carbon coating was applied to improve the electrochemical performance of $LiFePO_4$ cathodes. The chemical co-precipitation method was employed for the preparation of all the samples. XPS and EDX mapping proved that boron has been doped into the carbon coatings. Raman spectroscopy demonstrated that a high number of defects in the carbon-coated layer can be induced by boron. Thus, the electric conductivities of the $LiFePO_4$ samples coated by boron-doped carbon were greatly enhanced, and boron-doped modification was demonstrated to be an effective method.

2. Experimental

2.1. Materials and preparation

The chemical co-precipitation method was employed to prepare $LiFePO_4$ samples coated by boron-doped carbon. In a typical synthesis, $FeSO_4 \cdot 7H_2O$(Alfa, 99%), LiH_2PO_4 (Alfa,

[a]*Northwest Institute for Nonferrous Metal Research, Xi'an 710016, China. E-mail: wyf7777v @126.com*

[b]*State Key Laboratory for Mechanical Behavior of Materials, Xi'an Jiaotong University, Xi'an 710049, China*

97%) and $LiOH \cdot H_2O$ (Alfa, 98%) in stoichiometric amounts were chosen as starting materials. Glucose to a total weight of 20 wt% of the above chemicals was added into the aqueous solution as a carbon source. The suspension was stirred at 0–4 °C for about 30 min. The final precursor powder was then filtered, washed with ethanol, and dried at 100 °C in a vacuum oven for 2 h. Tris(pentafluorophenyl) borane ($C_{18}BF_{15}$), which was used as a boron source, was mixed with the precursor powder and ground for about 20 min. The $n(B)/n(C)$ percentages of $C_{18}BF_{15}$ and glucose were 0.1%, 0.3% and 0.5%, and the samples were labeled as $LiFePO_4/CB_{0.1}$, $LiFePO_4/CB_{0.3}$ and $LiFePO_4/CB_{0.5}$, respectively. Finally, the mixture was heat-treated at 975 K at Ar–H_2 atmosphere to synthesize the $LiFePO_4$/CB samples. For comparison, an undoped $LiFePO_4$/C sample was also prepared by a similar method without boron addition.

2.2. Characterization

The crystal and phase structures of the obtained samples were characterized by a D8 ADVANCE X-ray diffraction (XRD) instrument. Raman spectra were acquired by the Renishaw-Invia Raman system with an argon ion laser source (532 nm). XPS spectra were collected on a Escalab 250Xi instrument with a monochromatic Al K-alpha X-ray source. The precise content of boron was determined by inductively coupled plasma analysis using an IRIS Advantage ICP-AES spectrometer. SEM and TEM were performed to observe the particle morphology and size distribution. SEM images were taken on a JEOL JSM-6700 microscope at an accelerating voltage of 5 kV. The element mappings of the samples were characterized by JSM-6460 energy dispersive X-ray spectroscopy (EDX). TEM was performed on a JEOL JEM-2100 transmission electron microscope at an accelerating voltage of 200 kV. The phase and structure of the material were monitored using selected area electron diffraction (SAED). The carbon contents were accurately acquired with a Leco CS844 C-S analyzer.

2.3. Electrochemical measurement

The working electrode was prepared by casting a slurry of 86 wt% $LiFePO_4$/C or $LiFePO_4$/CB composites, 7 wt% carbon black and 7 wt% polyvinylidene fluoride (PVDF) binder on an aluminum foil as the current collector. Electrochemical performances of the as-prepared samples were studied using CR2025 coin-type cells, which consisted of a cathode, a Celgard separator and metallic lithium with 1 M $LiPF_6$ in EC/DEC (1 : 1 vol%) as the electrolyte. All the cells were assembled in an Ar-filled glove box (H_2O < 1 ppm, O_2 < 1 ppm). Galvanostatic cycling was measured on a Neware BTS Device between cut off voltages of 2.0 and 4.3 V (*vs.* Li/Li^+). Electrochemical impedance spectroscopy (EIS) was performed using an electrochemical work-station (CHI750) over the frequency range from 0.01 Hz to 100 kHz. Cyclic voltammetry (CV) testing was carried out at a scan rate of 0.1 mV s^{-1} between 2.0 and 4.3 V by CHI750. All the electrochemical measurements were performed at room temperature (25 °C).

3. Results and discussion

3.1. Structural and morphology characterization

The crystal and phase structures of all the samples were investigated by XRD analysis. As indicated in Fig. 1a, the samples were found to be pure $LiFePO_4$ with an ordered olivine structure (JCPDS card no. 83-2092), and they exhibited no impurities and a single phase. Carbon was not detected mainly because the residual carbon is amorphous. The amorphous carbon mostly originates from the decomposition product of glucose and slightly from the decomposition product of $C_{18}BF_{15}$.

Raman spectroscopy has historically been used to probe structural and electronic characteristics of graphite materials, thus providing useful information on the defects (D-band) and in-plane vibrations of sp^2 carbon atoms (G-band).[23,24] Raman spectra of all the samples in the wavenumber range of 1100–2000 cm^{-1} are shown in Fig. 1b. As we can see, the peaks of the D- and G-bands lie at about 1320 cm^{-1} and 1590 cm^{-1}, respectively. As we know, it is important to characterize defects by the intensity ratio of Raman D- and G-bands (I_D/I_G).[25,26] As illustrated in Fig. 1b, the I_D/I_G values for $LiFePO_4$/C, $LiFePO_4/CB_{0.1}$, $LiFePO_4/CB_{0.3}$ and $LiFePO_4/CB_{0.5}$ samples are 0.95, 1.13, 1.31 and 1.14, respectively. This confirms that many defects have been induced by boron doping, which will be helpful for electric conductivity, thus improving high-power capability of the cathodes.

To confirm that boron is doped into the carbon coatings, XPS analysis was conducted. The C 1s and B 1s spectra of the $LiFePO_4/CB_{0.3}$ sample are shown in Fig. 1c and d, respectively. The C 1s spectrum, as shown in Fig. 1c, exhibited a peak at about 284.9 eV, which agreed with previously reported results.[19,20] From the XPS spectrum of C 1s, the peaks at binding energies of 284.8 eV, 285.9 eV and 289.3 eV were assigned to sp^2 graphite C=C, C–O, and C=O bonds.[27,28] Moreover, a peak at about 282.7 eV could be assigned to the C–B species.[29] It is shown in Fig. 1d that the B 1s spectrum can be deconvoluted into three components: the peak at 188.6 eV corresponded to a BC_3-type bond,[30] and the peaks located at about 190.9 eV and 192.4 eV were assigned to BC_2O- and BCO_2-type bonds, respectively.[31,32] The above XPS analyses proved the doping of boron in this sample. For lithium-ion batteries, the graphite-like BC_3 dopant species plays a significant role in improving the electronic conductivity and electrochemical activity of the carbon-coated layer on the cathode surface.[19] It was confirmed that the $LiFePO_4$/CB composites exhibit better electrochemical properties than the undoped sample. To determine the precise content of boron in the resulting composites, ICP-AES analysis was employed, and a boron content of 0.16 wt% was detected for the $LiFePO_4/CB_{0.3}$ sample.

The morphology and dimensions of all the samples were characterized (Fig. 2) by SEM. The $LiFePO_4$/C sample showed spherical nano-grain morphology in the size range of 20–100 nm, as shown in Fig. 2a. This small grain size is beneficial for shortening the distance of lithium-ion migration, which enhances the migration rate of lithium ions. There are no visible differences among different samples (Fig. 3b–d) with

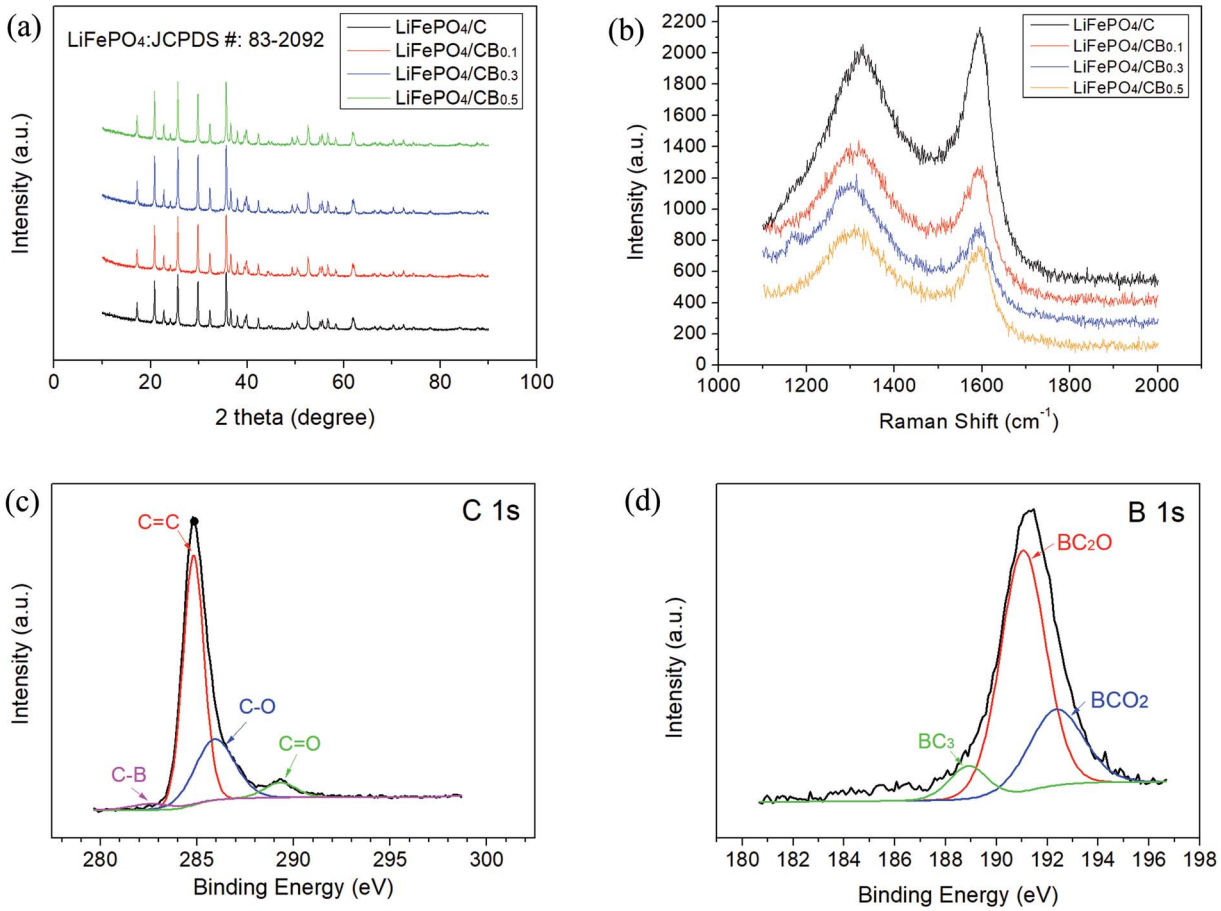

Fig. 1 (a) XRD patterns and (b) Raman spectra of the as-prepared $LiFePO_4$/C and various $LiFePO_4$/CB samples; XPS spectra of (c) C 1s and (d) B 1s for the $LiFePO_4/CB_{0.3}$ sample.

respect to morphologies and grain sizes. Fig. 3 shows SEM and EDX of the $LiFePO_4/CB_{0.3}$ sample. From the distribution of Fe, O, P, C and B (Fig. 3b–d), it can be confirmed that boron is homogenously distributed in all the samples.

The HRTEM images of all the samples are shown in Fig. 4. It can be seen that the carbon-coated layer is amorphous and about 2–4 nm in thickness. The thin carbon film is favorable for electronic transport during the electrochemical process. The SAED patterns are presented in the inset of Fig. 4. Both the SAED patterns and high-resolution lattice fringes reveal high crystallization in all the samples. It is also shown that diffraction spots have a tendency to become circular, as seen in the insets of Fig. 4c and d, which show random large angle crystallographic orientation among different grains. A C-S elemental analyzer is adopted to determine the carbon contents of all the samples. The measured results for $LiFePO_4$/C, $LiFePO_4/CB_{0.1}$, $LiFePO_4/CB_{0.3}$ and $LiFePO_4/CB_{0.5}$ samples are around 6.91%, 6.98%, 6.95% and 6.93%, respectively. This indicates that boron doping does not affect the carbon contents of the $LiFePO_4$ samples.

3.2. Dynamics and electrochemical performance

The electrochemical performances of all the samples were tested by coin cells. Fig. 5a exhibits the galvanostatic charge/discharge curves of different samples at a low rate of 0.5C. For all the cathodes, a planar platform at about 3.50 V is associated with the lithium-ion extraction process, and a flat discharge plateau at about 3.35 V corresponds to lithium-ion insertion into $LiFePO_4$ crystals. It can be observed from Fig. 5a that the $LiFePO_4$/C sample delivers an initial discharge capacity of 150.6 mA h g^{-1}, whereas the doped $LiFePO_4/CB_{0.1}$ and $LiFePO_4/CB_{0.3}$ samples exhibit higher discharge capacities than the $LiFePO_4$/C sample. Particularly, the $LiFePO_4/CB_{0.3}$ sample delivers the highest discharge capacity of 165.8 mA h g^{-1}. However, the $LiFePO_4/CB_{0.5}$ sample shows lower specific capacity, which may be caused by excess boron. The capacities of all the samples are calculated based on the content of $LiFePO_4$. The results for cycling performance combined with coulombic efficiency at 0.5C in the potential range of 2.0–4.3 V (Li^+/Li) are shown in Fig. 5b. All the samples show good cycling stabilities. As illustrated in Fig. 5b, there is nearly no degradation for all the samples during 200 discharge cycles at the rate of 0.5C. The coulombic efficiency approaches 88% for all the samples, as indicated in Fig. 5b. Particularly, the corresponding average coulombic efficiency for the $LiFePO_4/CB_{0.3}$ sample is above 99%, suggesting highly reversible Li-ion insertion/extraction kinetics.

To evaluate the effect of boron doping on lithium-ion migration into the bulk electrode and charge transfer

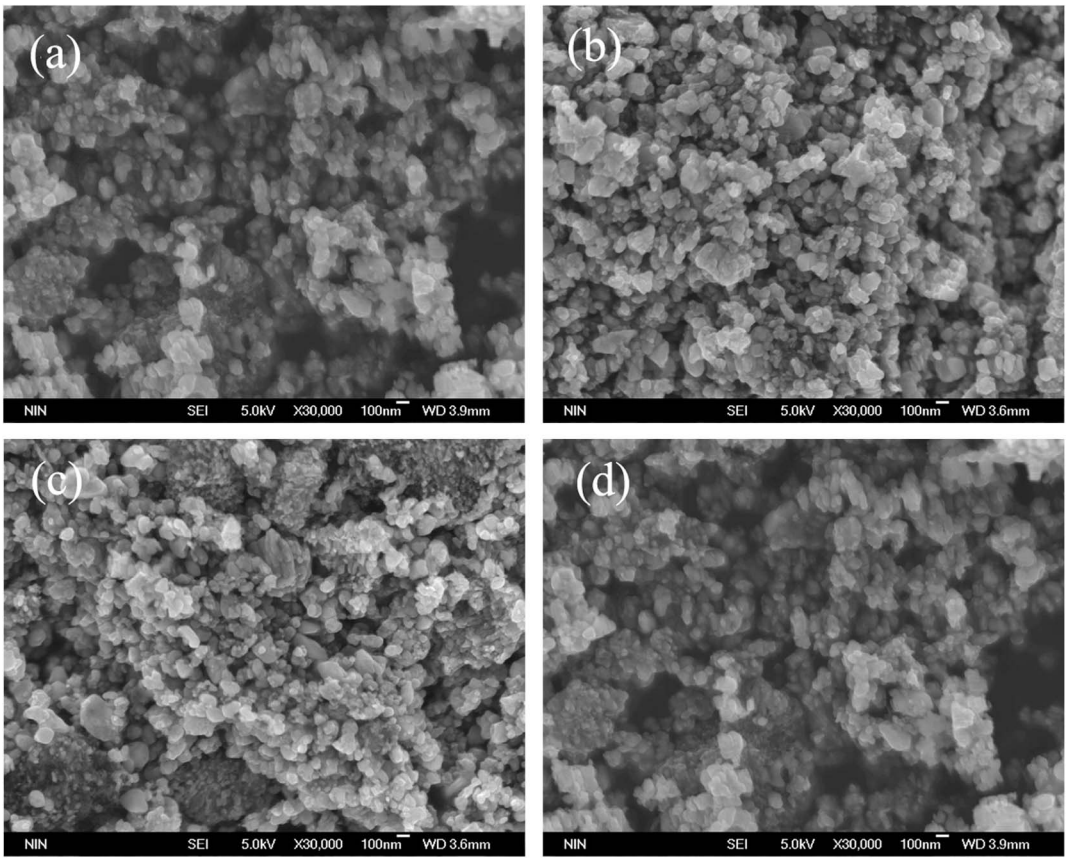

Fig. 2 SEM images of (a) $LiFePO_4/C$, (b) $LiFePO_4/CB_{0.1}$, (c) $LiFePO_4/CB_{0.3}$ and (d) $LiFePO_4/CB_{0.5}$ powders.

impedance, electrochemical impedance spectroscopy (EIS) of the cycled samples was carried out. Fig. 5c shows the EIS spectra of all the samples in the frequency range from 0.1 Hz to 100 kHz. All the EIS spectra clearly exhibit a semicircle in the high-to-middle frequency region and an inclined line within the low frequency range. The resistance of the semicircle corresponds

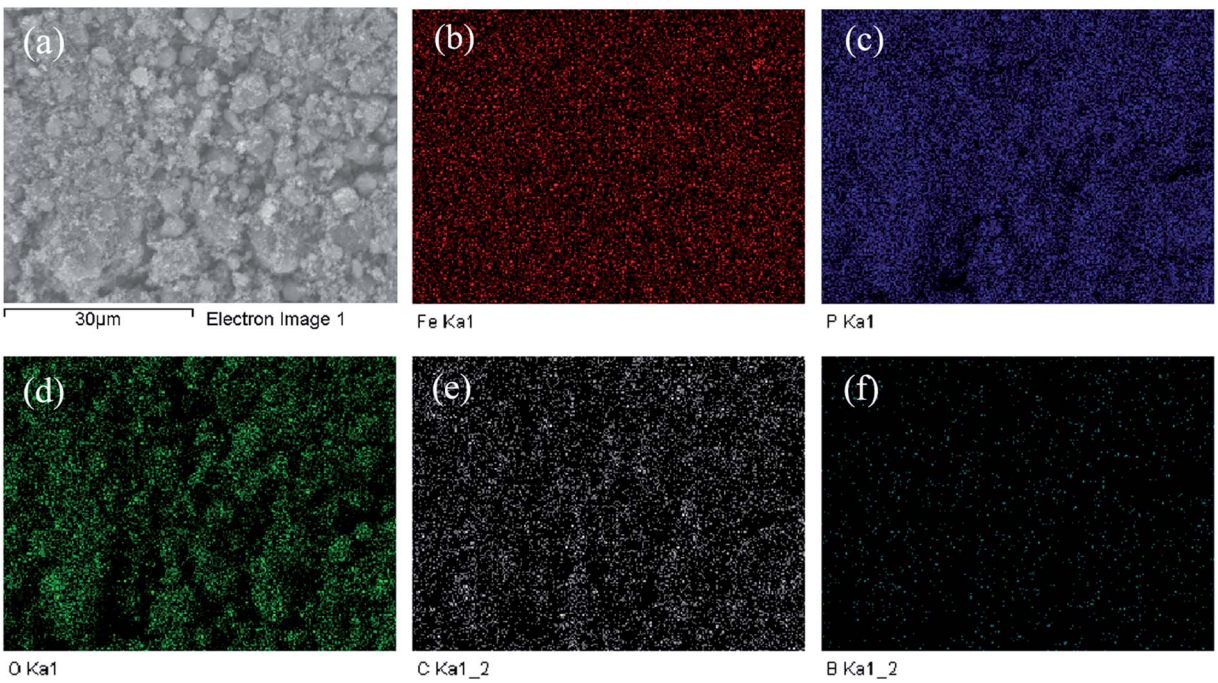

Fig. 3 (a) SEM image and (b–f) the corresponding EDX mapping images of $LiFePO_4/CB_{0.3}$.

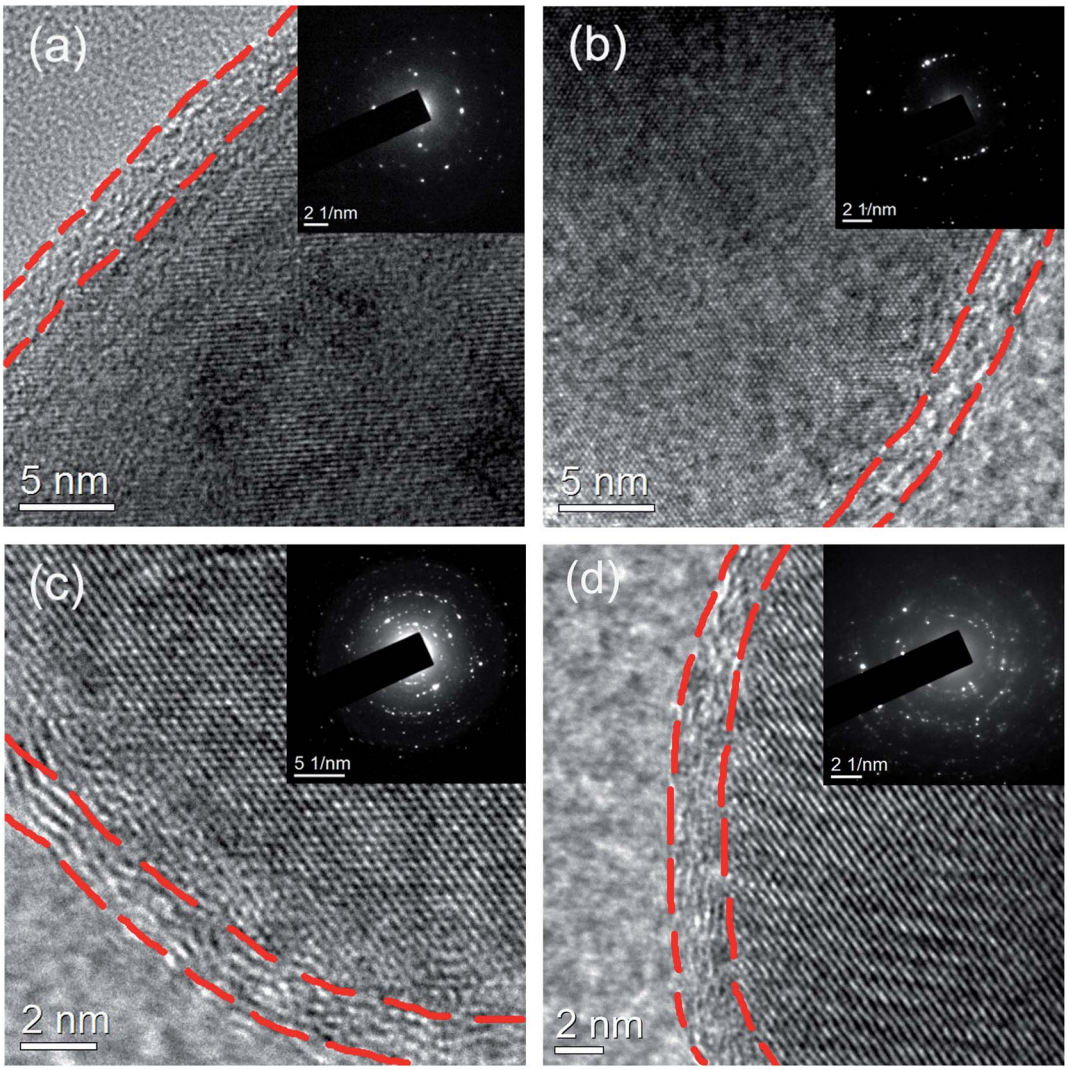

Fig. 4 HRTEM images of (a) $LiFePO_4$/C, (b) $LiFePO_4/CB_{0.1}$, (c) $LiFePO_4/CB_{0.3}$ and (d) $LiFePO_4/CB_{0.5}$ samples; the inset shows the SAED patterns of the samples.

to the charge-transfer process. Fig. 5c indicates that the charge transfer resistance is smaller for $LiFePO_4/CB_{0.1}$ and $LiFePO_4/CB_{0.3}$ samples than that for the $LiFePO_4$/C sample due to the smaller diameter of the semicircle. Therefore, suitable boron doping greatly enhances the conductivity of the cathodes and improves electron transport during the electrochemical charge/discharge process. The $LiFePO_4/CB_{0.5}$ sample shows higher charge-transfer resistance, which may be due to excess of boron.

The inclined line is assigned to the migration of lithium ions into the bulk of the electrode material, the so-called Warburg impedance (Z_w).[33] The Warburg coefficient (σ) can be obtained by the following eqn (1):[34]

$$Z_{re} = R_e + R_{ct} + \sigma\omega^{-1/2} \quad (1)$$

Here, R_e is the resistance of the electrolyte, R_{ct} is the charge transfer resistance and ω is the angular frequency in the low frequency region. Both R_e and R_{ct} are kinetic parameters that are independent of frequency. Thus, σ is the slope for the plot of Z_{re} *vs.* the reciprocal root square of the lower angular frequencies ($\omega^{-1/2}$). The plots of Z_{re} *vs.* the reciprocal root square of the lower angular frequencies ($\omega^{-1/2}$) at different levels of boron doping in $LiFePO_4$/C composites are shown in Fig. 5d. The slope of the fitted line is the Warburg coefficient σ. In addition, the Li-ion diffusion rates are determined by the following eqn (2):[35]

$$D = R^2T^2/2A^2n^4F^4C^2\sigma^2 \quad (2)$$

here, R is the gas constant, T is the absolute temperature (K), F is the Faraday constant, A is the surface area of the $LiFePO_4$ cathode, n is the number of electrons during the process of Li-ion transportation, C is the molar concentration of Li-ions in the $LiFePO_4$ cathode and σ is the Warburg coefficient. The Li-ion diffusion values are 2.32×10^{-13} cm^2 S^{-1}, 1.52×10^{-13} cm^2 S^{-1}, 1.32×10^{-13} cm^2 S^{-1} and 3.29×10^{-14} cm^2 S^{-1}, as determined by eqn (2) for the boron-doped nanocrystallized $LiFePO_4$/C, $LiFePO_4/CB_{0.1}$, $LiFePO_4/CB_{0.3}$ and $LiFePO_4/CB_{0.5}$ samples, respectively. It is noticed that the difference among the Li-ion diffusion rates is not much for the $LiFePO_4$/C,

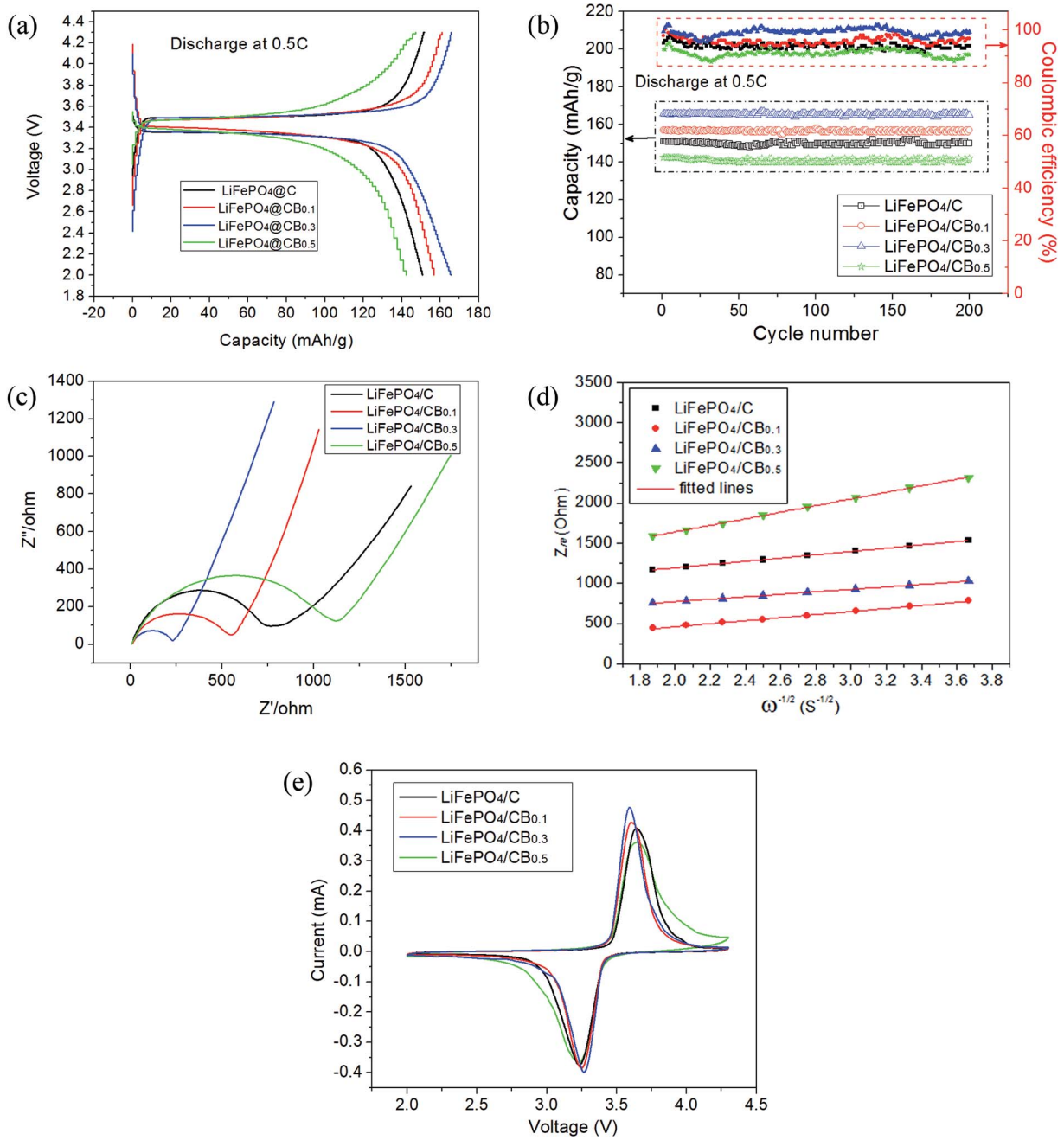

Fig. 5 Electrochemical behaviors of $LiFePO_4$/C and various $LiFePO_4$/CB electrodes: (a) initial specific capacities and (b) cycling performance combined with coulombic efficiency at 0.5C in the potential range of 2.0–4.3 V (Li^+/Li). (c) EIS spectrum after 50 cycles at 0.5C. (d) The plot of Z_{re} *vs.* the reciprocal root square of the lower angular frequencies ($\omega^{-1/2}$) at different amounts of boron doping in $LiFePO_4$/C composites. (e) CV curves at a scan rate of 0.1 mV s^{-1}.

$LiFePO_4/CB_{0.1}$ and $LiFePO_4/CB_{0.3}$ samples. Compared to the reported 10^{-13} to 10^{-16} in the literature,[36] the Li-ion diffusion rates of these nanocrystallized samples are improved due to short Li-transport lengths in $LiFePO_4$ and the coupling effects of electrons, since suitable boron doping notably increases the electric conductivity of $LiFePO_4$. Surplus boron doping hinders the transport of Li ions in $LiFePO_4$, which may be the reason for lower Li-ion diffusion rates in the $LiFePO_4/CB_{0.5}$ sample compared to those in other samples.

Cyclic voltammetry (CV) curves of $LiFePO_4$/C and various $LiFePO_4$/CB samples are measured at a scan rate of 0.1 mV s^{-1} and shown in Fig. 5e. It can be seen that a typical Fe^{3+}/Fe^{2+} redox couple corresponds to the $LiFePO_4/FePO_4$ two-phase reaction. It can be seen from Fig. 5e that the $LiFePO_4/CB_{0.3}$ sample delivers the lowest value of 321 mV in potential interval and the highest peak current intensity. This gives an index to the fastest kinetics of the electrons and lithium-ion migration of this sample. The

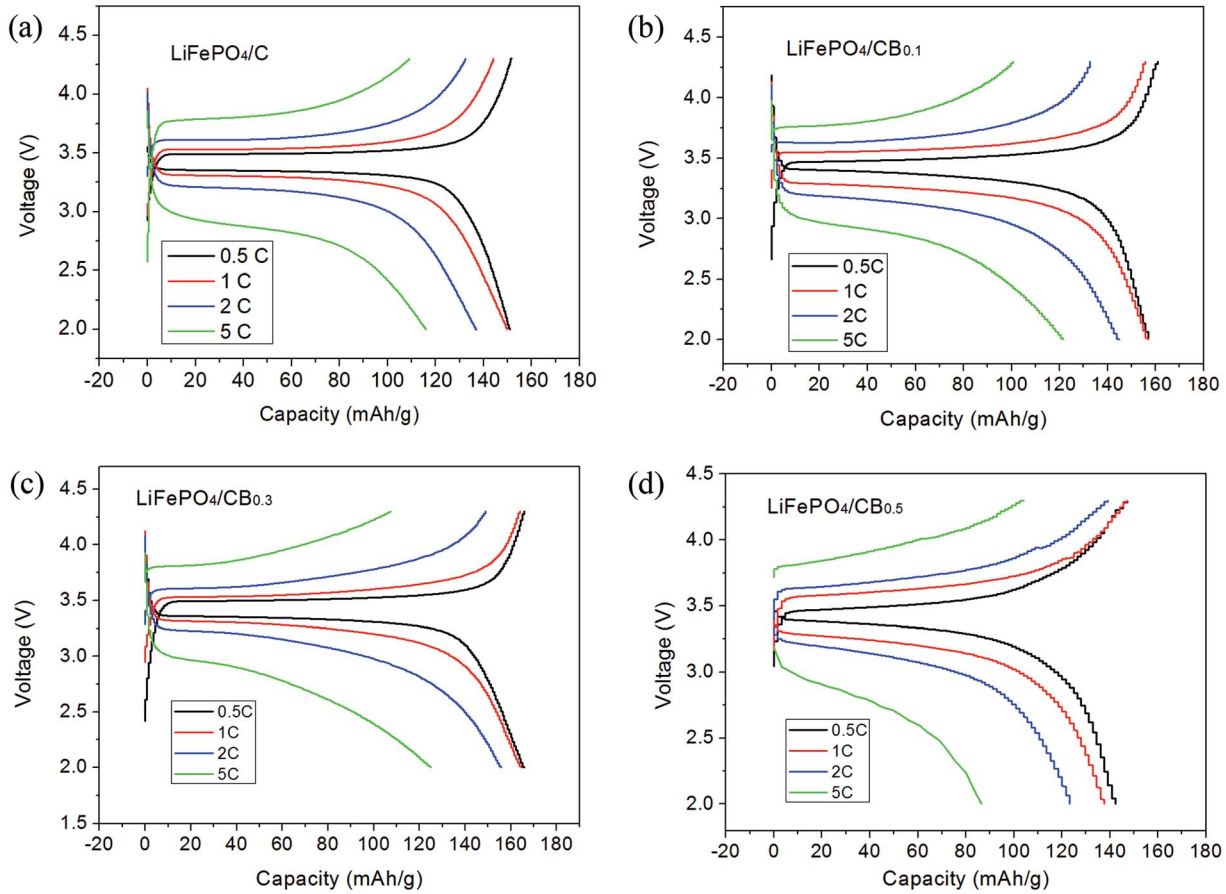

Fig. 6 The initial charge and discharge profiles of all the samples at rates from 0.1C to 5C at room temperature: (a) $LiFePO_4/C$, (b) $LiFePO_4/CB_{0.1}$, (c) $LiFePO_4/CB_{0.3}$ and (d) $LiFePO_4/CB_{0.5}$ samples.

above results match well with those of the galvanostatic electrochemical tests.

Fig. 6 exhibits the galvanostatic discharge/charge curves ranging from 0.5C to 5C between 2.0 V and 4.3 V for all the samples. As shown in Fig. 6a, the $LiFePO_4/C$ sample delivers higher discharge capacities of 150.9, 149.7, 136.9, and 116.0 mA h g^{-1} at 0.5C, 1C, 2C and 5C, respectively. It can be observed that the charge/discharge plateaus become uneven due to the electrode polarization as the rates increase. Compared to the specific discharge capacity of the undoped sample, the specific discharge capacities of the $LiFePO_4/CB_{0.1}$ and $LiFePO_4/CB_{0.3}$ electrodes first increase and then decrease for $LiFePO_4/CB_{0.5}$ electrodes, which may be caused by surplus boron addition. Of all the samples, the $LiFePO_4/CB_{0.3}$ sample exhibits the best high-rate capacity, maintaining 165.8 mA h g^{-1}, 164.4 mA h g^{-1}, 155.6 mA h g^{-1} and 124.8 mA h g^{-1} at 0.5C, 1C, 2C and 5C, respectively. The excellent high rate capacity of $LiFePO_4/CB_{0.3}$ cathode can be ascribed to doped boron, which may create new lithium active sites,[33] alter the electronic structure[37] and increase electric conductivity.[38]

4. Conclusion

Tris(pentafluorophenyl) borane ($C_{18}BF_{15}$) was successfully used as a boron source, and $LiFePO_4/CB$ composites were synthesized in this study. As the cathode material, the $LiFePO_4/CB_{0.3}$ sample exhibited a high specific capacity of 165 mA h g^{-1} and much improved rate capability of 124.8 mA h g^{-1} at a current rate of 5C. The analysis of EIS and CV tests revealed that the charge-transfer resistances of the cathodes clearly decreased by suitable boron doping, and the reversibilities of the electrode reactions were enhanced. This study indicates that the boron-doped $LiFePO_4/CB$ cathode is promising for high-power lithium-ion batteries.

Conflicts of interest

There are no conflicts of interest to declare.

Acknowledgements

This work was supported by National Natural Science Foundation of China (Grant no. 51504196) and Key Research and Development Plan of Shaanxi Province (Grant no. 2017ZDXM-GY-039).

References

1 Y. Meng, J. Xia, L. Wang, G. Wang, F. Zhu and Y. Zhang, A comparative study on $LiFePO_4/C$ by *in situ* coating with

different carbon sources for high-performance lithium batteries, *Electrochim. Acta*, 2018, **261**, 96–103.

2 X. Wang, Z. Feng, J. Huang, W. Deng, X. Li, H. Zhang and Z. Wen, Graphene-decorated carbon-coated $LiFePO_4$ nanospheres as a high-performance cathode material for lithium-ion batteries, *Carbon*, 2018, **127**, 149–157.

3 H. Raj and A. Sil, Effect of carbon coating on electrochemical performance of $LiFePO_4$ cathode material for Li-ion battery, *Ionics*, 2018, DOI: 10.1007/s11581-017-2423-0.

4 J. J. Wang and X. L. Sun, Understanding and recent development of carbon coating on $LiFePO_4$ cathode materials for lithium-ion batteries, *Energy Environ. Sci.*, 2012, **5**, 5163–5185.

5 Z. X. Chi, W. Zhang, F. Q. Cheng, J. T. Chen, A. M. Cao and L. J. Wan, Optimizing the carbon coating on $LiFePO_4$ for improved battery performance, *RSC Adv.*, 2014, **4**, 7795.

6 K. Okada, I. Kimuraa and K. Machida, High rate capability by sulfur-doping into $LiFePO_4$ matrix, *RSC Adv.*, 2018, **8**, 5848–5853.

7 J. Ma, B. H. Li, H. D. Du, C. J. Xu and F. Y. Kang, The improvement of the high-rate charge/discharge performances of $LiFePO_4$ cathode material by Sn doping, *J. Solid State Electrochem.*, 2012, **16**, 1–8.

8 K. L. Harrison, C. A. Bridges, M. P. Paranthaman, C. U. Segre, J. Katsoudas, V. A. Maroni, J. C. Idrobo, J. B. Goodenough and A. Manthiram, Temperature dependence of aliovalent-vanadium doping in $LiFePO_4$ cathodes, *Chem. Mater.*, 2013, **25**, 768–781.

9 C. Y. Nan, J. Lu, L. H. Li, L. L. Li, Q. Peng and Y. D. Li, Size and shape control of $LiFePO_4$ nanocrystals for better lithium ion battery cathode materials, *Nano Res.*, 2013, **6**, 469–477.

10 K. Kai, Y. Kobayashi, H. Miyashiro, G. Oyama, S. Nishimura, M. Okubo and A. Yamada, Particle-size effects on the entropy behavior of a Li_xFePO_4 electrode, *ChemPhysChem*, 2014, **15**, 2156–2161.

11 J. Shi, X. Zhang, X. Zhang and Y. Xiang, Titania and nitrogen-doped carbon co-modification: Their synergic effects on the electrochemical performance of $LiFePO_4$, *J. Alloys Compd.*, 2018, **750**, 139–146.

12 B. Han, X. D. Meng, L. Ma and J. Y. Nan, Nitrogen-doped carbon decorated $LiFePO_4$ composite synthesized *via* a microwave heating route using polydopamine as carbon–nitrogen precursor, *Ceram. Int.*, 2016, **42**, 2789–2797.

13 S. L. Chen, Q. L. Tang, X. H. Chen and L. Y. Tan, Nitrogen-doped carbon coated $LiFePO_4$/carbon nanotube interconnected nanocomposites for high performance lithium ion batteries, *New J. Chem.*, 2015, **39**, 9782–9788.

14 K. Okada, I. Kimura and K. Machida, High rate capability by sulfur-doping into $LiFePO_4$ matrix, *RSC Adv.*, 2018, **8**, 5848–5853.

15 C. Wang, Z. Y. Guo, W. Shen, A. L. Zhang, Q. J. Xu, H. M. Liu and Y. G. Wang, Application of sulfur-doped carbon coating on the surface of $Li_3V_2(PO_4)_3$ composites to facilitate Li-ion storage as cathode materials, *J. Mater. Chem. A*, 2015, **3**, 6064–6072.

16 D. Xu, P. F. Wang and B. W. Shen, Synthesis and characterization of sulfur-doped carbon decorated $LiFePO_4$ nanocomposite as high performance cathode material for lithium-ion batteries, *Ceram. Int.*, 2016, **42**, 5331–5338.

17 J. L. Zhang, J. Wang, Y. Y. Liu, N. Nie, J. J. Gu, F. Yu and W. Li, High-performance lithium iron phosphate with phosphorus-doped carbon layers for lithium ion batteries, *J. Mater. Chem. A*, 2015, **3**, 2043–2049.

18 X. L. Su, T. Huang, Y. G. Wang and A. S. Yu, Synthesis and electrochemical performance of nano-sized $Li_4Ti_5O_{12}$ coated with boron-doped carbon, *Electrochim. Acta*, 2016, **196**, 300–308.

19 C. Wang, Z. Y. Guo, W. Shen, Q. J. Xu, H. M. Liu and Y. G. Wang, B-doped carbon coating improves the electrochemical performance of electrode materials for Li-ion batteries, *Adv. Funct. Mater.*, 2014, **24**, 5511–5521.

20 W. Shen, H. Li, C. Wang, Z. H. Li, Q. J. Xu, H. M. Liu and Y. G. Wang, Improved electrochemical performance of the $Na_3V_2(PO_4)_3$ cathode by B-doping of the carbon coating layer for sodium-ion batteries, *J. Mater. Chem. A*, 2015, **3**, 15190–15201.

21 C. E. Lowell, Solid solution of boron in graphite, *J. Am. Ceram. Soc.*, 1967, **50**, 142–144.

22 Y. F. Zhan, J. L. Huang, Z. P. Lin, X. Yu, D. R. Zeng, X. X. Zhang, F. Y. Xie, W. H. Zhang, J. Chen and H. Meng, Iodine/nitrogen co-doped graphene as metal free catalyst for oxygen reduction reaction, *Carbon*, 2015, **95**, 930–939.

23 Y. F. Zhan, J. L. Huang, Z. P. Lin, X. Yu, D. R. Zeng, X. X. Zhang, F. Y. Xie, W. H. Zhang, J. Chen and H. Meng, Iodine/nitrogen co-doped graphene as metal free catalyst for oxygen reduction reaction, *Carbon*, 2015, **95**, 930–939.

24 Z. S. Wu, A. Winter, L. Chen, Y. Sun, A. Turchanin, X. L. Feng and K. Mullen, Three-dimensional nitrogen and boron co-doped graphene for high-performance all-solid-state supercapacitors, *Adv. Mater.*, 2012, **24**, 5130–5135.

25 Y. Yan, Y. X. Yin, S. Xin, Y. G. Guo and L. J. Wan, Ionothermal synthesis of sulfur-doped porous carbons hybridized with graphene as superior anode materials for lithium-ion batteries, *Chem. Commun.*, 2012, **48**, 10663–10665.

26 Y. S. Yun, V. D. Le, H. Kim, S. J. Chang, S. J. Baek, S. Park, B. H. Kim, Y. H. Kim, K. Kang and H. J. Jin, Effects of sulfur doping on graphene-based nanosheets for use as anode materials in lithium-ion batteries, *J. Power Sources*, 2014, **262**, 79–85.

27 L. Yang, S. Liang, Y. Zhao, L. Zhu, S. Chen, X. Wang, Q. Wu, J. Ma, Y. Ma and Z. Hu, Boron-doped carbon nanotubes as metal-free electrocatalysts for the oxygen reduction reaction, *Angew. Chem., Int. Ed.*, 2011, **50**, 7132–7135.

28 M. Cattelan, S. Agnoli, M. Favaro, D. Garoli, F. Romanato, M. Meneghetti, A. Barinov, P. Dudin and G. Granozzi, Microscopic view on a chemical vapor deposition route to boron-doped graphene nanostructures, *Chem. Mater.*, 2013, **25**, 1490–1495.

29 Y. B. Tang, L. C. Yin, Y. Yang, X. H. Bo, Y. L. Cao, H. E. Wang, W. J. Zhang, I. Bello, S. T. Lee, H. M. Cheng and C. S. Lee, Tunable band gaps and p-type transport properties of

boron-doped graphene by controllable ion doping using reactive microwave plasma, *ACS Nano*, 2012, **6**, 1970–1978.

30 J. Ozaki, N. Kimura, T. Anahara and A. Oya, Preparation and oxygen reduction activity of BN-doped carbons, *Carbon*, 2007, **45**, 1847–1853.

31 G. Jo and S. Shanmugam, Single-step synthetic approach for boron-doped carbons as a non-precious catalyst for oxygen reduction in alkaline medium, *Electrochem. Commun.*, 2012, **25**, 101–104.

32 Y. Zhao, L. Yang, S. Chen, X. Wang, Y. Ma, Q. Wu, Y. Jiang, W. Qian and Z. Hu, Can boron and nitrogen co-doping improve oxygen reduction reaction activity of carbon nanotubes?, *J. Am. Chem. Soc.*, 2013, **135**, 1201–1204.

33 Y. Zhao, L. Yang, S. Chen, X. Wang, Y. Ma, Q. Wu, Y. Jiang, W. Qian and Z. Hu, Can boron and nitrogen co-doping improve oxygen reduction reaction activity of carbon nanotubes?, *J. Am. Chem. Soc.*, 2013, **135**, 1201–1204.

34 Y. Cui, X. Zhao and R. Guo, Improved electrochemical performance of $La_{0.7}Sr_{0.3}MnO_3$ and carbon co-coated $LiFePO_4$ synthesized by freeze-drying process, *Electrochim. Acta*, 2010, **55**, 922–926.

35 L.-l. Wang, P.-h. Ma, K. Zhang, C.-h. Gao and C.-y. Yan, Determination of Li-ion Diffusion Coefficient *via* Coulometric Titration and Electrochemical Impendence Method, *J. Salt Lake Res.*, 2009, **17**, 52–55.

36 Z. Wei-Jun, Structure and performance of $LiFePO_4$ cathode materials: A review, *J. Power Sources*, 2011, **196**, 2962–2970.

37 J. Han, L. L. Zhang, S. Lee, J. Oh, K. S. Lee, J. R. Potts, J. Ji, X. Zhao, R. S. Ruoff and S. J. Park, Generation of B-doped graphene nanoplatelets using a solution process and their supercapacitor applications, *ACS Nano*, 2012, **7**, 19–26.

38 Y. A. Kim, K. Fujisawa, H. Muramatsu, T. Hayashi, M. Endo, T. Fujimori, K. Kaneko, M. Terrones, J. Behrends, A. Eckmann, C. Casiraghi, K. S. Novoselov, R. Saito and M. S. Dresselhaus, Raman spectroscopy of B-doped single-layer graphene, *ACS Nano*, 2012, **6**, 6293–6300.